Journal of Nuclear Materials 394 (2009) 136–143

Contents lists available at ScienceDirect

Journal of Nuclear Materials

journal homepage: www.elsevier.com/locate/jnucmat

An analytical study on the effects of strain gradient on the fracture statistics of quasi-brittle materials

Haiyan Li *, Alex Siu-Lun Fok

Minnesota Dental Research Center for Biomaterials and Biomechanics, School of Dentistry, University of Minnesota, USA

ARTICLE INFO

Article history:
Received 13 March 2009
Accepted 26 August 2009

ABSTRACT

A deterministic model with material strain-softening has been employed to predict the failure process of quasi-brittle materials subjected to different strain gradients. The failures of beams in pure bending and L-shape specimens in tension are simulated using this model, and the influence of material damage rate on the failure process is studied. The effect of statistical variations in the material properties on the fracture statistics of the components is then considered. The model correctly predicts the changes in the magnitude and distribution of the failure loads of specimens with different strain gradients. The results can help explain the influence of strain gradient on the fracture statistics of quasi-brittle materials.

1. Introduction

Predicting the failure of components made of brittle or quasi-brittle materials, such as graphite, ceramics and concrete, has been a challenging task for materials scientists and engineers. Because of the heterogeneity inherent in the microstructure, the material properties, notably the strength, of brittle materials usually have very large variations. Therefore, in the design or safety assessment of brittle components, probabilistic models such as that of Weibull's are usually adopted [1–3].

The two-parameter Weibull probabilistic model can be expressed as:

$$P_f = 1 - \exp\left[-\int_V \left(\frac{\sigma}{\sigma_0}\right)^m \frac{dV}{V}\right], \tag{1}$$

where P_f is the failure probability, σ is the applied stress, σ_0 is related to the mean strength per unit volume of the material, m is a reciprocal measure of the variation in the material's strength, and V is the volume of the component. σ_0 and m are usually called the Weibull parameters, and are often taken to be material constants.

The Weibull model is often used to explain the so-called size-effect [4] on the strength of brittle materials – the bigger the component, the lower the strength – because of the higher probability of the existence of a strength-limiting flaw in larger components. Similarly, the model can explain the difference between the tensile and bend strength of brittle materials. According to the theory, because of the smaller effective stressed volume of a beam in bending, as compared to that in tension, the bend strength of a brittle material is on average higher than its tensile strength.

However, there is evidence showing that the Weibull parameters are in fact not material constants, being dependent on the stress state and geometry of the component. For example, both the Weibull modulus and mean volumetric fracture strength of graphite under biaxial flexure have been found to be higher than those under uniaxial flexure [5,6]. For silicon nitride, Kawamoto et al. [7] reported higher Weibull modulus for the bend strength than for the tensile strength. Similar results have been reported by Price [8] on nuclear graphite. Changes in the Weibull parameters of brittle materials also appear to be more pronounced with increasing strain gradient. Fig. 1 shows significant increases in the Weibull modulus of the fracture load of some graphite L-shaped specimens with increasing stress concentration at the notch [9].

More importantly, the Weibull model seriously underestimates the mean failure strength of components with high stress concentrations because of the particular form of the Weibull stress function [10], as given in Eq. (1). A nonlocal approach using spatial averaging of the stresses has been proposed by Bazant and Novak [4] to overcome this problem, but this seems to contradict with the weakest-link theory on which the Weibull model is based. Also, the problem with the dependence of the Weibull parameters on stress state and specimen shape still remains, and the predictions given by the Weibull model are rather sensitive to its parameters [2].

The strain-softening behaviour of quasi-brittle materials has been shown by many workers to be an alternative, deterministic explanation for the difference between the tensile and flexural strength of such materials [11]. Using the finite element method and a fictitious crack model, Hillerborg et al. [12] considered the ratio between bending and tensile strength of concrete beams with different beam depths. Good agreement between theory and experiments was obtained. Raphael [13] and Bazant and Li [14]

* Corresponding author. Tel.: +1 612 626 2556; fax: +1 612 626 1484.
E-mail address: lixx0775@umn.edu (H. Li).

0022-3115/$ - see front matter © 2009 Elsevier B.V. All rights reserved.
doi:10.1016/j.jnucmat.2009.08.017

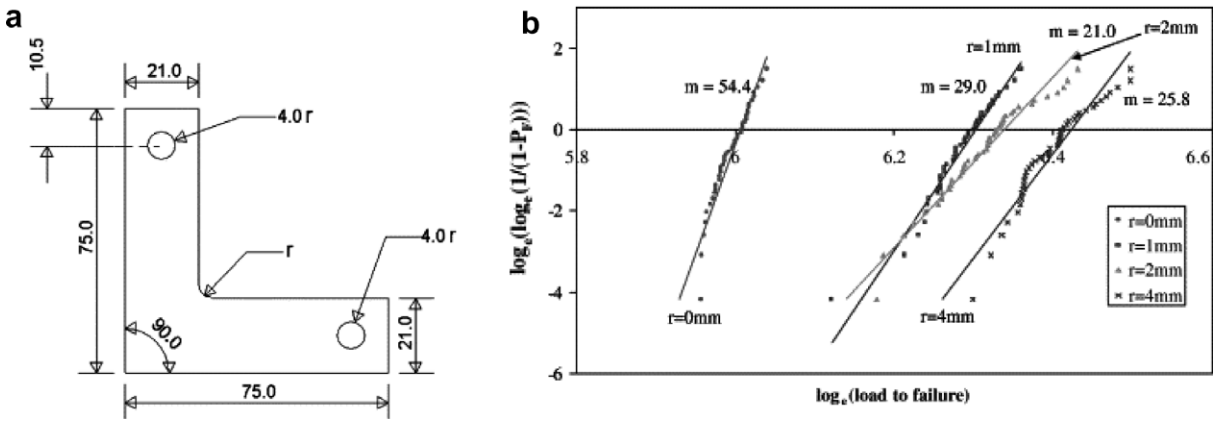

Fig. 1. (a) Dimensions of L-shaped specimen and (b) Weibull plots from testing L-shaped specimens with different corner radii.

used nonlinear stress–strain continuum models to investigate the same problem and obtain similar results. The latter workers concluded that the size-effect on the flexural strength of concrete was caused by the strain gradient within the beams. A similar conclusion on size-effect was drawn by van Vliet and van Mier [15] who conducted a series of uniaxial tension experiments on concrete. They further showed that the strain gradients were caused by the specimen shape, load eccentricity and material heterogeneity.

The aim of this paper is to show that, in addition to causing changes in the mean strength, strain gradients can also cause changes in the spread, i.e. Weibull modulus, of the failure loads of brittle components. Using a strain-softening material model, the failures of bars in uniform tension, beams in pure bending and specimens with different degrees of stress concentration were deterministically predicted. A Monte Carlo analysis was then performed by randomly changing the failure strain to investigate the effect of stress concentration on the spread of the failure loads of nominally identical specimens. It will be shown that, not only can the strain-softening material model explain deterministically the difference between the tensile and flexural strengths of brittle materials, it can also correctly predict changes in the spread of the failure loads of brittle components with different strain gradients. The current results should therefore be useful for improving the accuracy of failure predictions for brittle materials using a probabilistic approach.

2. Material behaviour

Fig. 2 shows a typical stress–strain curve for quasi-brittle materials [15,16]. The behaviour is initially linear and elastic, but after reaching a critical strain value, the material will then soften and ultimately fracture. In this study, following the approach by Bazant and Li [14], such behaviour is modelled by the simplified bilinear stress–strain curve in Fig. 3b (model B), where ε_{cr} is the critical strain and ε_u is the ultimate failure strain. For comparison purposes, an ideally brittle model with no strain-softening prior to fracture, as shown in Fig. 3a (model A), is also considered. The difference between these two material models can also be illustrated by the different forms of the elastic modulus as a function of strain, as shown in Fig. 4a and b, respectively. For material model B, the elastic modulus as a function of strain has the form:

$$\begin{cases} E = E_0, & \varepsilon \leqslant \varepsilon_{cr}, \\ E = E_0\varepsilon_{cr}(\varepsilon_u - \varepsilon)/(\varepsilon_u - \varepsilon_{cr})/\varepsilon, & \varepsilon_{cr} < \varepsilon \leqslant \varepsilon_u, \\ E = 0, & \varepsilon > \varepsilon_u. \end{cases} \tag{2}$$

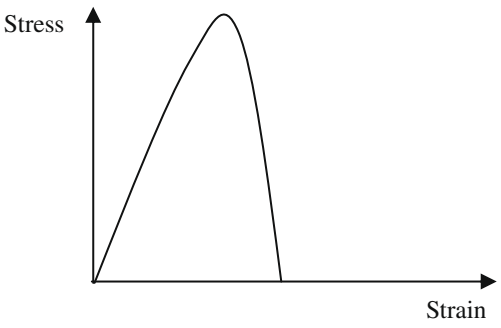

Fig. 2. A typical stress strain curve of quasi-brittle materials.

3. Beam in pure bending

For a beam of depth d and breadth b under pure bending, the applied bending moment M can be determined by integrating the first moment of the longitudinal direct stress σ along the beam depth, i.e.

$$\begin{aligned} M &= \int_0^d b \cdot \sigma(\varepsilon) \cdot y dy, \\ &= \int_0^d b \cdot E(\varepsilon) \cdot \varepsilon(y) \cdot y dy, \end{aligned} \tag{3}$$

where E is the elastic modulus, which is a function of the applied strain as indicated in Fig. 4 and Eq. (2).

The loading process is divided into three stages according to the maximum strain, ε_0, at the top tensile surface of the beam. The three loading stages are: (1) before material damage ($\varepsilon_0 < \varepsilon_{cr}$), (2) after damage initiation but before crack formation ($\varepsilon_{cr} < \varepsilon_0 < \varepsilon_u$), and (3) crack formation and propagation ($\varepsilon_0 > \varepsilon_u$). For simplicity, the distribution of strain ε across the beam depth is assumed to be linear throughout the entire loading process [7,9], i.e.

$$\varepsilon = \varepsilon_c + (\varepsilon_0 - \varepsilon_c)\frac{y}{d}, \tag{4}$$

where ε_c is the strain on the compressive face. Further, material damage and crack propagation are assumed to occur along a single vertical crack path. The strain and stress distributions along the crack path for the three loading stages are shown schematically in Fig. 5a–c, respectively. Note that, since brittle materials are much stronger in compression than in tension, compressive stresses or strains are assumed not to cause material damage or failure.

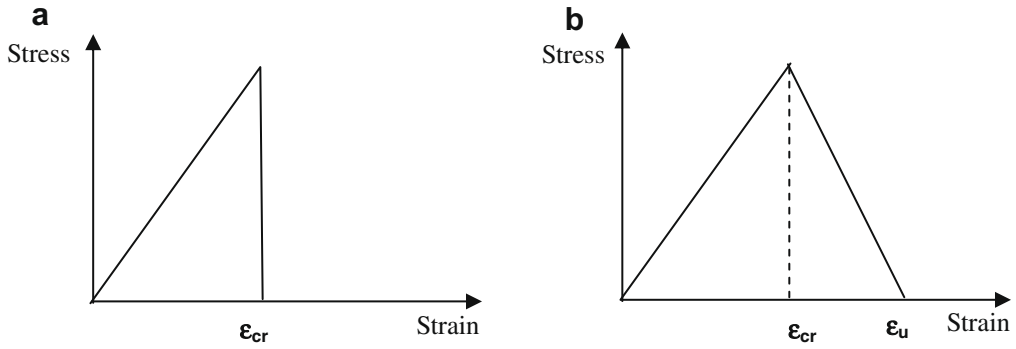

Fig. 3. Idealised stress–strain curves of (a) material model A without strain-softening and (b) material model B with strain-softening prior to fracture.

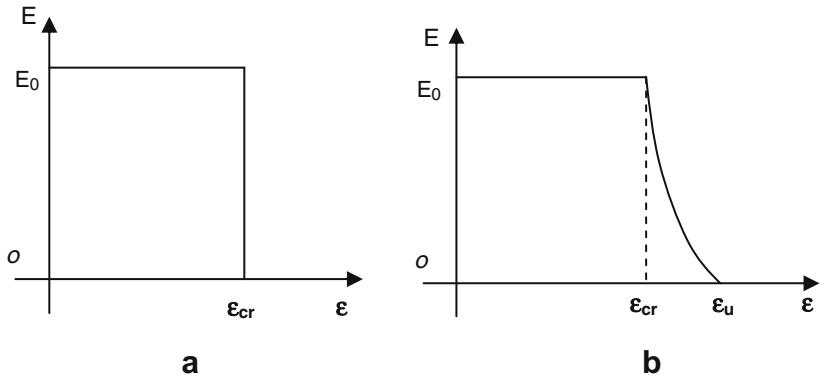

Fig. 4. Young's modulus against strain curves: (a) material model A and (b) material model B.

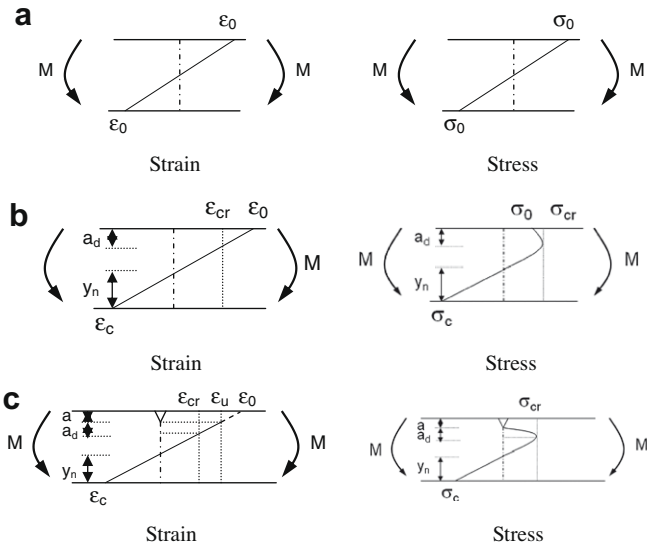

Fig. 5. Strain and stress distributions of brittle beam under pure bending: (a) before material damage ($\varepsilon_0 < \varepsilon_{cr}$), (b) during material damage but prior to cracking ($\varepsilon_{cr} < \varepsilon_0 < \varepsilon_u$), and (c) during crack propagation ($\varepsilon_0 > \varepsilon_u$).

When $\varepsilon_0 < \varepsilon_{cr}$ (Fig. 5a), since all the materials are linearly elastic, the moment M can be easily derived from Eqs. (3) and (4) as a function of the maximum tensile strain ε_0.

When $\varepsilon_0 > \varepsilon_{cr}$ or $\varepsilon_0 > \varepsilon_u$ (Fig. 5b and c), because of material softening and/or cracking at the top surface, the position of the neutral axis y_n will shift downward. To obtain the moment M using Eq. (3), the position of the neutral axis y_n, the length of the damage zone a_d, and the compressive strain ε_c at the bottom surface will need to be determined first according to the equilibrium condition:

$$\int_0^d b \cdot \sigma \cdot dy = \int_0^d b \cdot E(\varepsilon) \cdot \varepsilon(y) \cdot dy = 0, \tag{5}$$

since the beam is in pure bending. Note that the three unknowns y_n, a_d and ε_c are related through similar triangles (see Fig. 5), so Eq. (5) can be made to contain one unknown only and is thus solvable to give a unique solution.

The strain at the cracked portion of the cross-section is of course indeterminate. It is used here to represent the average or effective strain over the length of the beam at that position.

The technical computing language software Matlab [17] was used to first solve numerically Eq. (5) and then calculate the applied moment using Eq. (3). Figs. 6 and 7 show the predicted equivalent stress ($6M/bd^2$) based on simple beam theory against the maximum surface strain for the beam in pure bending using the two material models illustrated in Figs. 3 and 4. The stress for a bar under uniform tension using the same material models are also given for comparison. The dimensions and material parameters used were: $b = 10$ mm, $d = 20$ mm, $E = 10$ GPa, $\varepsilon_{cr} = 0.002$ and $\varepsilon_u = 1.5\varepsilon_{cr}$.

It can be clearly seen from Figs. 6 and 7 that, with material model A, the predicted tensile strength and flexural strength are the same. However, with material model B, which softens gradually prior to fracture, the predicted flexural strength is higher than the tensile strength.

The difference between the tensile and flexural strengths depends on the difference between ε_{cr} and ε_u. By increasing the ultimate failure strain, ε_u, Fig. 8 shows that, for the bar in tension, only the failure strain has been increased; the failure stress remains the same. For the beam in bending, however, both the nominal failure

stress and failure strain have been increased by an increase in the ultimate failure strain of the material. For the particular material model considered, a 30% increase in ε_u results in approximately

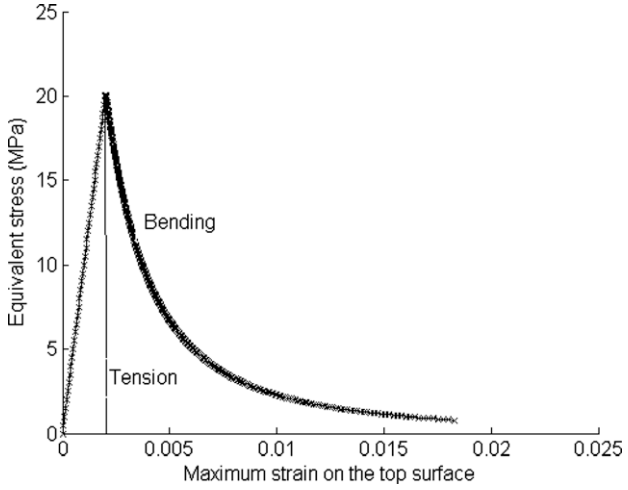

Fig. 6. Equivalent stress against maximum surface strain using material model A.

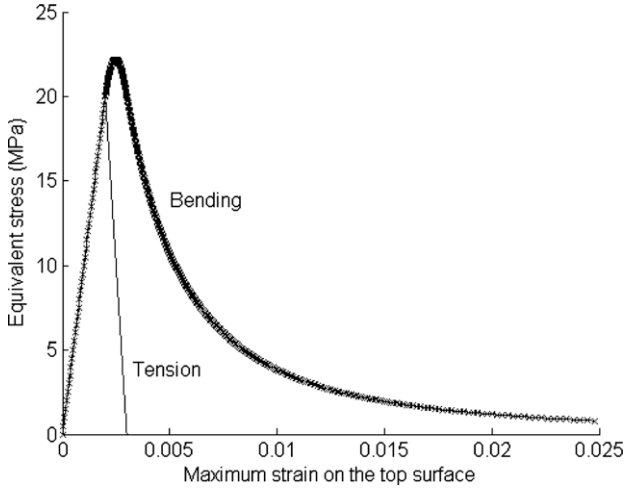

Fig. 7. Equivalent stress against maximum surface strain using material model B.

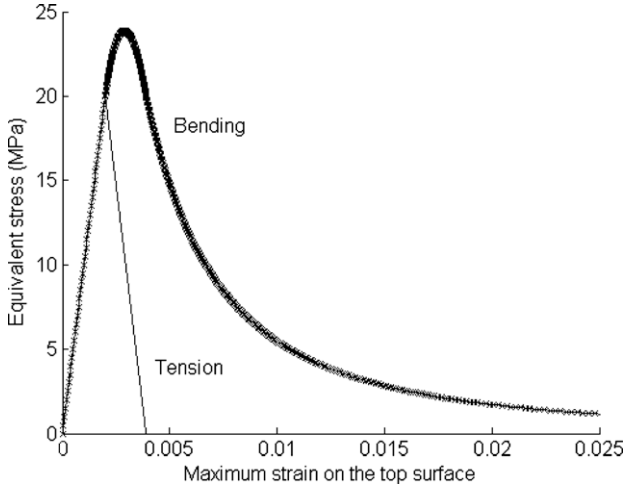

Fig. 8. Equivalent stress against maximum surface strain with 30% increase in ε_u.

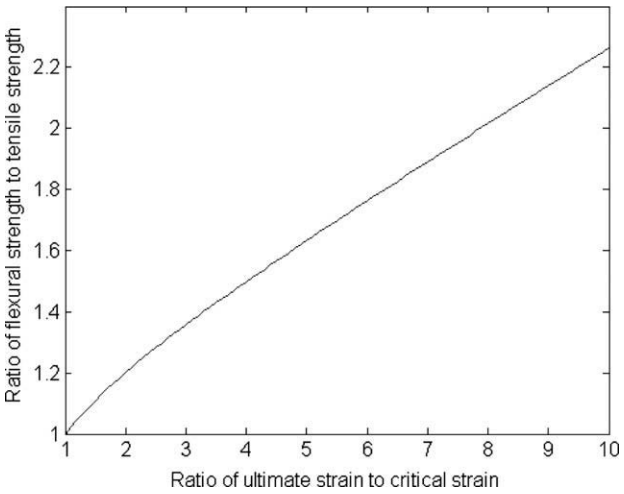

Fig. 9. Ratio of flexural to tensile strength against ratio of ε_u to ε_{cr}.

10% increase in the flexural strength. Fig. 9 shows the ratio of flexural strength to tensile strength against the ratio of ultimate strain to critical strain, $\varepsilon_u/\varepsilon_{cr}$, based on a critical strain $\varepsilon_{cr} = 0.002$.

4. Components with a high stress concentration

For components with a high stress concentration, such as the L-shaped specimen in tension shown in Fig. 1a, the strain distribution along the crack path is approximated by a power function of the form (Fig. 10):

$$\varepsilon = \varepsilon_0 \left(\frac{y}{d}\right)^n, \tag{6}$$

where ε_0 is the maximum strain at the inner corner point, d is the length of the crack path, y is the distance along the crack path, and n is a parameter governing the shape of the strain distribution or degree of strain concentration. It is assumed that the smaller the corner radius of the specimen, the larger the value of n, and higher the strain concentration.

The applied tensile load P can be expressed as:

$$P = \int_0^d b \cdot \sigma(\varepsilon) \cdot dy = \int_0^d b \cdot E(\varepsilon) \cdot \varepsilon \cdot dy, \tag{7}$$

where b is the thickness of the specimen.

The whole loading and fracture process is again divided into three stages according to the maximum strain ε_0: (1) before material damage ($\varepsilon_0 < \varepsilon_{cr}$), (2) after damage initiation but before crack formation ($\varepsilon_{cr} < \varepsilon_0 < \varepsilon_u$), and (3) crack formation and propagation ($\varepsilon_0 > \varepsilon_u$). The strain and stress distributions along the crack path of the specimen for the three loading stages are shown schematically

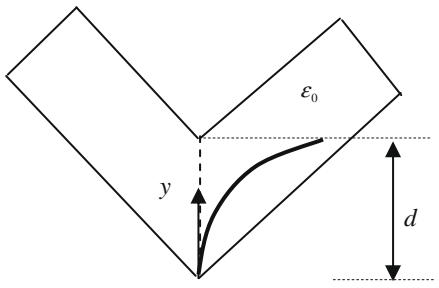

Fig. 10. Schematic strain distribution along the crack path of the L-shaped specimen under tension.

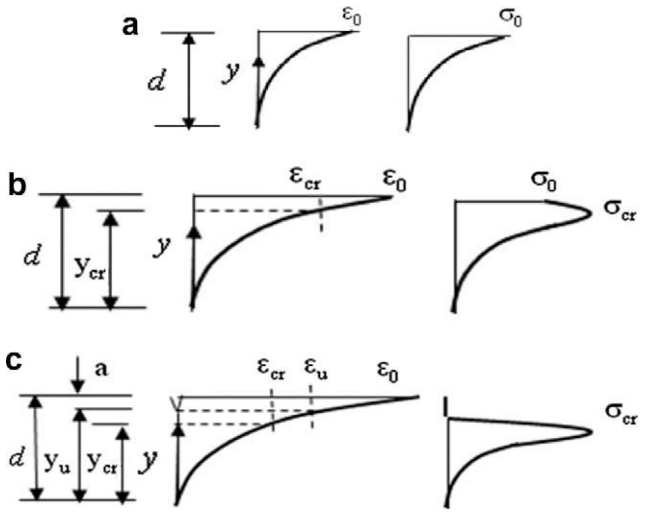

Fig. 11. Strain and stress distributions of L-shaped specimen under tension: (a) before material damage ($\varepsilon_0 < \varepsilon_{cr}$), (b) during material damage but prior to cracking ($\varepsilon_{cr} < \varepsilon_0 < \varepsilon_u$), and (c) during crack propagation ($\varepsilon_0 > \varepsilon_u$).

in Fig. 11a–c, respectively. ε_0 is taken to be the independent variable, and the tensile load P is determined at each stage of loading as a function of ε_0.

4.1. Applied load for stage 1 – before material damage ($\varepsilon_0 < \varepsilon_{cr}$)

During this stage of loading, the material is linearly elastic, and its Young's modulus has a constant value of E_0. The applied load, P_1, can be obtained by substituting Eq. (6) into (7) and integrating. Thus,

$$P_1 = \int_0^d b \cdot E_0 \cdot \varepsilon_0 \left(\frac{y}{d}\right)^n \cdot dy, \\ = \frac{b \cdot d \cdot E_0 \varepsilon_0}{n+1}. \tag{8}$$

4.2. Applied load for stage 2 – after damage initiation but prior to cracking ($\varepsilon_{cr} < \varepsilon_0 < \varepsilon_u$)

During this stage of loading, there is material softening which initiates at the inner corner of the specimen. The stress distribution along the crack path can be separated into two parts: the elastic portion up to the critical stress $\sigma_{cr} = E_0\varepsilon_{cr}$ and the strain-softening portion where $\varepsilon > \varepsilon_{cr}$; see Fig. 11b. The depth of material without damage, y_{cr}, is a function of ε_{cr} and ε_0:

$$y_{cr} = d \cdot \left(\frac{\varepsilon_{cr}}{\varepsilon_0}\right)^{\frac{1}{n}}, \tag{9}$$

and the applied load for this stage of loading, P_2, can be expressed:

$$P_2 = \int_0^{y_{cr}} b \cdot E_0 \cdot \varepsilon_0 \left(\frac{y}{d}\right)^n \cdot dy + \int_{y_{cr}}^d b \cdot E(\varepsilon) \cdot \varepsilon_0 \left(\frac{y}{d}\right)^n \cdot dy. \tag{10}$$

4.3. Applied load for stage 3 – crack formation and propagation ($\varepsilon_0 > \varepsilon_u$)

When the maximum strain is greater than the ultimate failure strain, ε_u, a crack is assumed to appear at the inner corner. The resulting distributions of strain and stress are shown in Fig. 11c, in which a is the crack length, y_{cr} and y_u are the remaining depths of material with strains lower than ε_{cr} and ε_u, respectively. y_{cr} can again be obtained using Eq. (9), while y_u and a are:

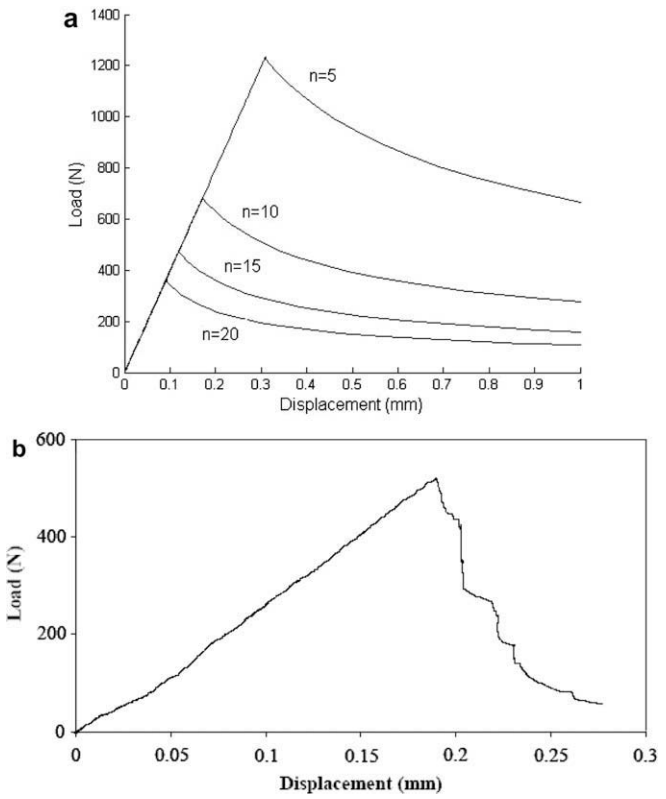

Fig. 12. (a) Predicted load–displacement curves for L-shaped specimens with different values of n for the strain distribution, Eq. (6). (b) Experimental load–displacement curve of L-shaped specimen with a corner radius of 2 mm [18].

$$y_u = d \cdot \left(\frac{\varepsilon_u}{\varepsilon_0}\right)^{\frac{1}{n}}, \tag{11}$$

and

$$a = d - y_u, \tag{12}$$

respectively. Thus, the load, P_3, after crack formation is given as:

$$P_3 = \int_0^{y_{cr}} b \cdot E_0 \cdot \varepsilon_0 \left(\frac{y}{d}\right)^n \cdot dy + \int_{y_{cr}}^{y_u} b \cdot E(\varepsilon) \cdot \varepsilon_0 \left(\frac{y}{d}\right)^n \cdot dy. \tag{13}$$

Material model B (Figs. 3b and 4b) was considered for this case. The parameters assumed were: $b = 15$ mm, $d = 21$ mm, $E_0 = 10$ GPa, $\varepsilon_{cr} = 0.002$ and $\varepsilon_u = 1.5\varepsilon_{cr}$. These are based on the properties of medium grained semi-isotropic extruded graphite tested in Refs. [9,18].

Fig. 12a gives the predicted load against displacement curves for different n values. The displacement in Fig. 12a is estimated approximately from the load P according to simple beam theory, with the uncracked section being used as the effective beam depth. It can be seen that with an increase of n, i.e. a steeper strain gradient or a smaller corner radius, the failure load decreases. The failure process is also more gradual, with possibly stable crack propagation, for cases with very high stress/strain gradients. These observations are in accord with the experimental results presented in Ref. [18] (see Fig. 12b), and are similar to those seen in the compact tensile test [19].

5. Statistical analysis

With the above analytical model, statistical analysis can be easily conducted with an assumed statistical distribution of the critical strain ε_{cr}. Fig. 13 shows such a distribution based on the

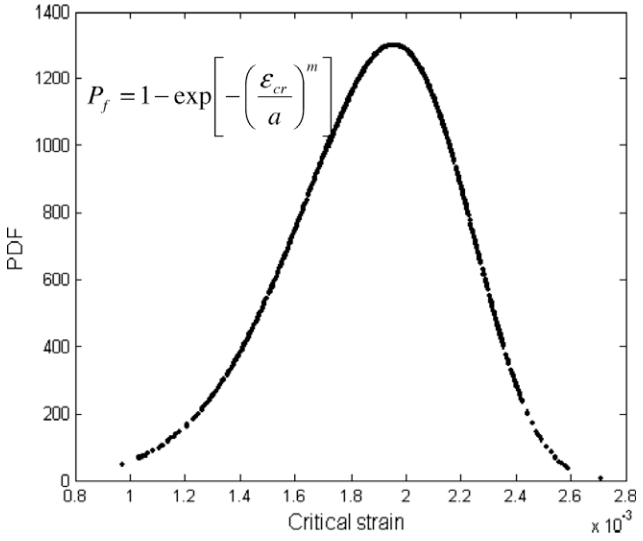

Fig. 13. Weibull distribution of critical strain (a = 0.2%, m = 7).

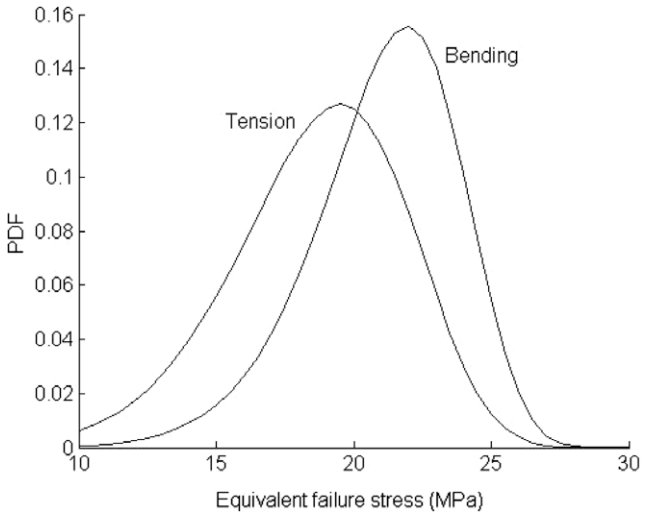

Fig. 15. PDF of equivalent failure stress using material model B, assuming constant ε_u.

Weibull function with a normalizing strain of 0.2% and a Weibull modulus of 7. The number of samples used was 3000, which were randomly created by Matlab.

5.1. Beams in pure bending

Figs. 14 and 15 give the probability distribution function (PDF) of the equivalent failure stress of bars under tension and beams in bending, using material models A and B (Fig. 3), respectively. For illustration, the critical strain was assumed to follow the Weibull distribution as shown in Fig. 13, while the ultimate strain ε_u was assumed to be a constant, i.e. 1.5 times the mean critical strain. When the ideally brittle material model A is used, the statistical distributions of the failure stress are the same for both bending and tension, and follow the shape of the critical strain distribution. However, when gradual material softening is considered, i.e. using material model B, the statistical distribution of the failure stress of beams under bending becomes different from that of the bars in tension. The bars in tension have a lower mean value but a wider spread in their strengths. The beams under bending, on the other hand, have a higher mean value but a narrower spread in their strengths.

Fig. 16 gives the Weibull failure probability plots for the bars in tension and beams in bending using material model B. The results again demonstrate the statistical difference between the two stress states. Not only are the two curves separated by the difference in their mean strengths, their slopes are also different, indicating a dependence of the spread on the stress state. The Weibull moduli m for tension and bending are 6.9 and 9.4, respectively. Note that the same trend has been reported for graphite and silicon nitride [7–9].

5.2. Components with a high stress concentration

Figs. 17 and 18 show the PDF and Weibull plots of the failure loads of specimens with their concentrated strain distributions represented by Eq. (6). It can be seen that with the increase of n, the mean failure load reduces while the Weibull modulus m increases. These are, again, consistent with the experimental results presented in [10,18] for graphite; see Fig. 1b.

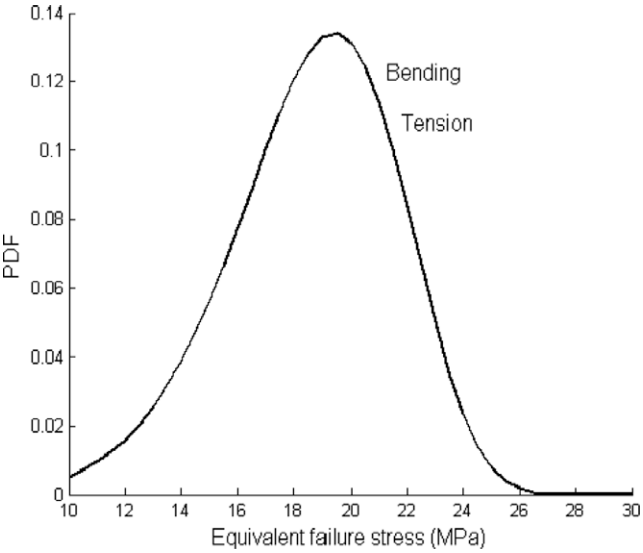

Fig. 14. PDF of equivalent failure stress using material model A.

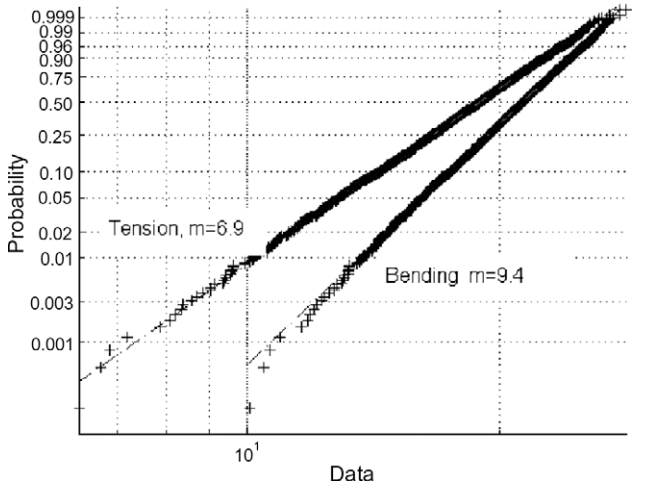

Fig. 16. Weibull failure plots of bar in tension and beam in bending using material model B, assuming constant ε_u.

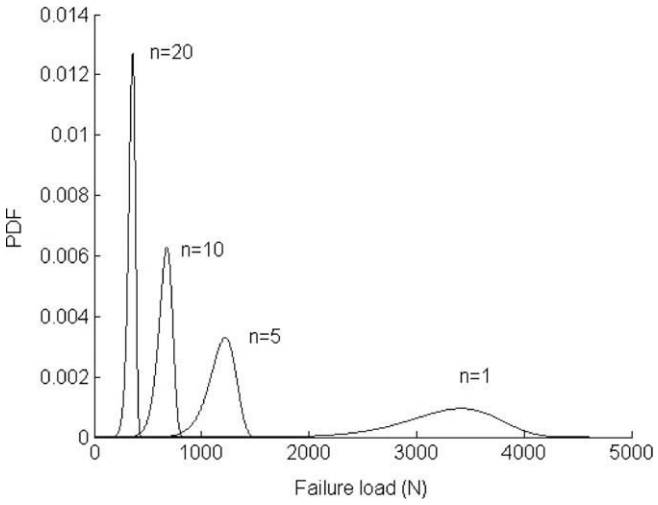

Fig. 17. PDF of failure load of L-shaped specimens with different strain gradients.

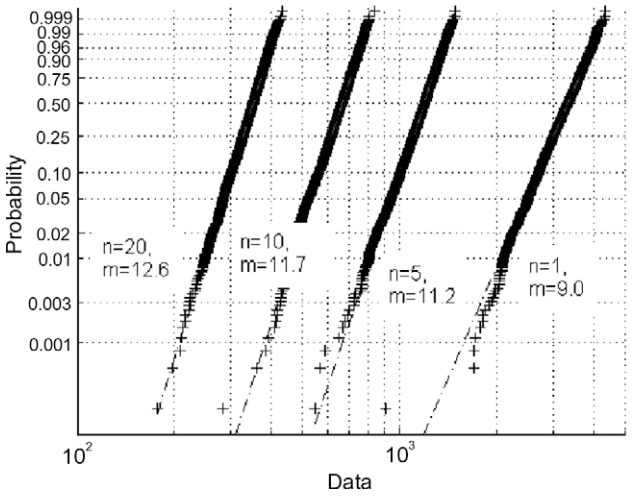

Fig. 18. Weibull failure plots of L-shaped specimens with different strain gradients, assuming constant ε_u.

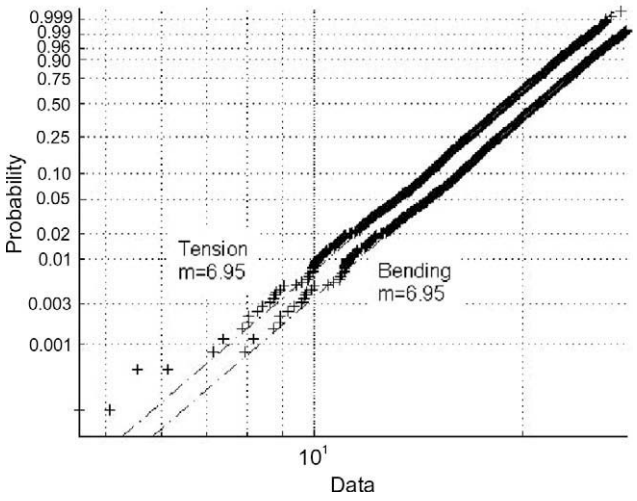

Fig. 19. Weibull failure plots of bar in tension and beam in bending, assuming $\varepsilon_u = 1.5\varepsilon_{cr}$.

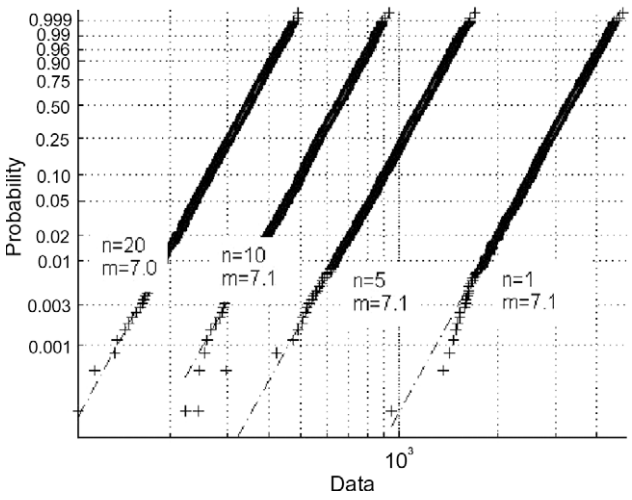

Fig. 20. Weibull failure plots of L-shaped specimen with different strain gradients, assuming $\varepsilon_u = 1.5\varepsilon_{cr}$.

5.3. Sensitivity to ε_u

The above results are all based on the assumption that the ultimate strain ε_u is a constant (1.5 times the mean critical strain) and only the critical strain ε_{cr} has a statistical distribution. For the case where ε_u changes with ε_{cr} according to the ratio $\varepsilon_u = 1.5\varepsilon_{cr}$, the predicted results for the bars and beams and for the specimens with a high stress concentration are shown in Figs. 19 and 20, respectively. It can be seen that the Weibull modulus m is now almost insensitive to the strain gradient. The corresponding changes in the mean failure load are also smaller.

6. Discussion

Using a simple constitutive model, the dependence on the strain gradient of the magnitude and spread of the failure loads of quasi-brittle components has been considered. The numerical predictions are qualitatively in good agreement with the experimental results reported by other investigators.

The assumption of linear strain distribution within the beam in bending for all stages of loading is perhaps too simplistic, especially after crack formation. This can be improved by using more realistic strain distributions which can be obtained with the help of full-field strain measurement techniques such as electronic speckle pattern interferometry (ESPI) or numerical stress analysis. As for the material model, the bilinear stress–strain curves used may also be too simplistic and further refinement may be required. However, the assumption of linear strain distribution for the uncracked section has recently been used by Wu et al. [20] to predict the effective fracture toughness of concrete notched beams under 3-point bending, and good agreement between predictions and experiments has been obtained. The main difference between the current work and that of Wu et al. [20] is that the current work uses an approximate continuum approach with nonlinear stress–strain behaviour to model the damage process zone, while Wu et al. [20] use the fictitious crack model. In any case, the linear strain distribution assumption is probably valid up to the point of peak load prior to crack formation, and the post-peak behaviour will not affect the subsequent statistical analysis on the spread of the peak loads.

Despite the simplifications, the analytical method presented in this paper is still capable of producing very representative results. Notably, it predicts deterministically a flexural strength higher than the tensile strength – as seen in experiments on all kinds of

brittle materials – when the material model with strain-softening is used. When the ideally brittle material model is used, however, there is no difference between the flexural and tensile strengths. The apparent increase in the failure stress of brittle beams under bending is therefore due to the ability of the material to sustain further increase in load even after damage initiation up to the point of critical load. This is similar to the effect of plasticity in metallic materials which can continue to provide significant resistance to loading even after yielding.

The simple analytical model also successfully reproduces the shape of the load–displacement curve of the graphite L-shape specimen and the reduction of its failure (peak) load with decreasing corner radius. However, the predicted applied load beyond the peak value only approaches zero asymptotically, leading to overestimates of the load for very large prescribed displacements, especially for specimens with low stress concentrations or n values. Note that, just as in the beam under bending, the strain distribution is expected to change significantly after crack formation. Specifically, the strain concentration will become more pronounced (increased n value), and all the L-shape specimens are expected to have similar post-failure load–displacement characteristics because of the now similar strain concentrations, irrespective of their initial notch radius. It is expected that using more realistic strain distributions and more representative strain-softening material models will improve the load predictions. However, as stated above, the post-peak behaviour should not influence the statistical analysis on the spread of the peak loads.

It is worth pointing out that the predicted failure loads presented in this work agree qualitatively with those given by previous finite element analyses for nuclear graphite using the more sophisticated continuum damage mechanics (CDM) model [21,22]. For example, it was found that, with the CDM model, an 'elastic-perfectly plastic' behaviour was essential in providing a flexural strength higher than the tensile strength [22]. This agreement is perhaps not surprising since the approach taken here is similar to the CDM model. The current work, however, provides a more fundamental understanding to the previous numerical predictions and the actual failure process that takes place in quasi-brittle materials.

The simple analytical model allows statistical and sensitivity analysis to be performed readily to account for the inherent variations in the properties of brittle materials. It correctly predicts the change in the spread of the failure loads of specimens with different strain gradients; specifically, the increase in the Weibull modulus with increased stress concentration. At the same time, by changing the relationship between the critical and ultimate strains of the material, there is sufficient flexibility in the model to capture different statistical behaviours. For quasi-brittle materials such as graphite and ceramics, it seems that the constant ultimate strain assumption is more appropriate as it correctly predicts a higher Weibull modulus in bending than in tension. More sophisticated analysis can be carried out using finite element models with randomly distributed material properties [23]. However, the computational effort required is far more extensive.

An intuitive explanation is offered here for the change in Weibull modulus with strain gradient. For brittle components with a low stress concentration, e.g. the bar in tension, failure of the components is caused by the unstable propagation of the most critical flaw. The weakest-link theory would therefore be appropriate for these components. On the other hand, for brittle components with a high stress concentration, gross failure is often preceded by the stable propagation and coalescence of several or even many subcritical flaws. Using the throwing of dice as an analogy, when there is only one die, the numbers 1–6 will have a uniform probability distribution. When there are more than one dice, however, the probability distribution for the sum of the numbers from the dice will have a peak in the middle. For example, with two dice, the possible outcomes are 2, 3, 4, ..., 12, but the probability distribution will peak at the number 7. Similarly, it is reasonable to expect brittle components with a higher stress concentration to have a narrower spread in their failure loads because of their dependence on the combined failure of more than one flaws.

7. Conclusions

- A simple deterministic failure model based on nonlinear stress–strain curves has been employed for predicting the failure of quasi-brittle materials. The model correctly predicts the failure behaviour of specimens with different strain gradients, including those with high stress concentrations.
- A flexural strength higher than the tensile strength is predicted when a material model with gradual strain-softening is considered. The effect is similar to that of plasticity in metals in providing load resistance even after material damage has initiated.
- The numerical results agree qualitatively with those predicted using the more sophisticated FE-based continuum damage mechanics (CDM) model.
- The model, though deterministic in nature, can incorporate statistical effects readily. The increase in the Weibull modulus of the failure loads with increasing strain gradients has been correctly predicted.

Acknowledgements

This study was supported by the Grant-in-Aid program of the University of Minnesota. The authors would like to acknowledge the Minnesota Supercomputing Institute (MSI) for providing the computing services for this study.

References

[1] N. McLachlan, R.T. Szczepura, M.A. Davies, R.C.B. Judge, B.J. Marsden, Nucl. Energy 35 (1) (1996) 15.
[2] S.L. Fok, B.C. Mitchell, J. Smart, B.J. Marsden, Eng. Fract. Mech. 68 (2001) 1171.
[3] Q.S. Li, J.Q. Fang, D.K. Liu, J. Tang, Cem. Concr. Res. 33 (2003) 1631.
[4] Z.P. Bazant, D. Novak, J. Eng. Mech. 126 (2) (2000) 166.
[5] P. Stanley, C. Karroum, J. Strain Anal. 27 (1992) 101.
[6] J. Smart, S.L. Fok, Determining Failure Laws for Ceramic Materials, ASME Paper 94-GT-85, 1994.
[7] H. Kawamoto, T. Shimizu, M. Suzuki, H. Miyazaki, Strength analysis of Si_3N_4 swirl chamber for high power turbocharged diesel engines, Presented at the Second International Symposium on Ceramic Materials and Components for Engines, Lubeck-Travemurde, West Germany, April 1986.
[8] R.J. Price, Statistical Study of the Strength of Near-isotropic Graphite, GA Report GA-A13955, May 24, 1976.
[9] B.C. Mitchell, J. Smart, S.L. Fok, B.J. Marsden, J. Nucl. Mater. 322 (2003) 126.
[10] J. Smart, The failure of graphite channel sections, in: Proceedings of the International Conference on Computer Aided Assessment and Control of Localized Damage, vol. 3, Computational Mechanics Publications, 1990.
[11] J. Zhang, Mag. Concr. Res. 58 (9) (2006) 609.
[12] A. Hillerborg, M. Modeer, P.E. Petersson, Cem. Concr. Res. 6 (1976) 773.
[13] J.M. Raphael, ACI J. 81 (1984) 158.
[14] Z.P. Bazant, Z. Li, J. Struct. Eng. 121 (4) (1995) 739.
[15] R.A. van Vliet Marcel, G.M. van Mier Jan, Int. J. Fract. 95 (1999) 195.
[16] S. Popovics, Cem. Concr. Res. 3 (1973) 583.
[17] Duane C. Hanselman, Mastering MATLAB 6, 2001.
[18] B. Mitchell, The Understanding and Development of Nuclear Graphite Technology, PhD Thesis, The University of Manchester, 2003.
[19] P. Ouagne, G.B. Neighbour, B. McEnaney, J. Phys. D: Appl. Phys. 35 (2002) 927.
[20] Z. Wu, S. Yang, X. Hu, J. Zheng, Eng. Fract. Mech. 73 (2006) 2166.
[21] Z. Zou, S.L. Fok, S.O. Oyadiji, B.J. Marsden, J. Nucl. Mater. 324 (2004) 116.
[22] L. Shi, H. Li, S.L. Fok, B.J. Marsden, The effect of softening on the predicted strength of brittle materials using a continuum damage mechanics failure model, in: Second International Topical Meeting on High Temperature Reactor Technology, Beijing, 2004.
[23] J.M. Berthelot, L. Fatmi, Eng. Fract. Mech. 71 (2004) 1535.